



## Size-structure dynamics of the rotifer chemostat: a simple physiologically structured model

James N. McNair<sup>1</sup>, Martin E. Boraas<sup>2</sup> & Dianne B. Seale<sup>2</sup>

<sup>1</sup>*Patrick Center for Environmental Research, The Academy of Natural Sciences of Philadelphia, 1900 Benjamin Franklin Parkway, Philadelphia, PA 19103, U.S.A.*

<sup>2</sup>*Department of Biological Sciences, University of Wisconsin at Milwaukee, P.O. Box 413, Milwaukee, WI 53201, U.S.A.*

**Key words:** population dynamics, size structure, dilution rate

### Abstract

The classical chemostat models of Monod and others were designed for unicellular organisms. We summarize evidence that these models are not adequate for the rotifer chemostat, then propose a new, physiologically structured model that resolves some of their key problems yet remains biologically simple. The new model includes separate ontogenetic stages for eggs and free-swimming rotifers, with generalized age structure in the egg stage and body mass structure in the free-swimming stage. We present several numerical examples to illustrate the model's behavior, and we compare these in a preliminary way with experimental evidence from the literature.

### Introduction

Current knowledge of the principles of population dynamics is unsatisfactory on both empirical and theoretical grounds. The main problems are a weak empirical base, overly simple models with but vague links to real systems, and little effective interplay between theory and experiment. We therefore believe there is a need for renewed emphasis on carefully controlled laboratory studies of population dynamics, and on the development of structured population models that can be related clearly, directly, and convincingly to real experimental systems.

The rotifer chemostat is an excellent system for conducting laboratory population-dynamics studies. Relevant experimental techniques, concepts, and sample data are outlined in a companion paper (Boraas et al., 1998). Here we summarize the basic ideas underlying classical models of the chemostat, show that these models are inadequate for rotifers, and outline a new model that we believe has the potential to provide a more satisfactory theory.

### Classical chemostat models

The main component of the rotifer chemostat is an enclosed culture vessel containing a suspension of rotifers and algae (Figure 1A). The culture is kept well mixed to maintain spatial homogeneity. Fresh algal suspension (from an algal chemostat) is pumped into the culture at a continuous, regulated rate. Since the culture volume is fixed, outflow exactly balances inflow (dimensions: volume·time<sup>-1</sup>). The culture vessel is kept in the dark (to minimize algal growth and division) under tightly controlled physical conditions and is monitored regularly. (See Boraas et al., 1998, for additional details.)

In attempting to characterize the rotifer chemostat mathematically, previous studies have employed models originally developed for unicellular organisms, including Monod's (1950) model and a few straightforward variants. We refer to these collectively as classical chemostat models. A typical example is the Monod-Herbert model (Herbert, 1958), which differs from Monod's model simply by permitting loss of biomass via catabolism.

All classical chemostat models assume that the state of a rotifer population at any time  $t$  can be ad-

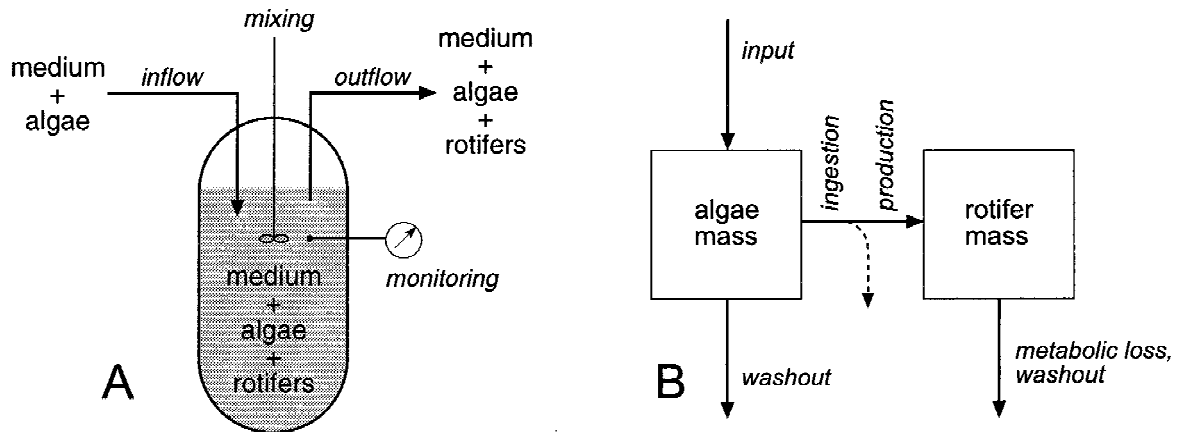


Figure 1. A—Basic components of the rotifer chemostat (highly schematic). See text for description, and Boraas et al. (1998) for additional details. B—Schematic of the Monod-Herbert model. See text for description.

equately characterized by a single number  $M(t)$ , which usually is some measure of the total mass of the population (e.g. total carbon). The dynamics of  $M(t)$  are assumed to be determined by the difference between the rate at which total rotifer biomass grows (as a result of ingesting algae and converting it into rotifer biomass) and the rates at which total rotifer biomass is diminished by catabolism and by being washed out of the chemostat. Similarly, it is assumed that the state of the algae population can be adequately characterized by a single number representing its total mass, whose dynamics are determined by the difference between the rate at which algal biomass is fed into the chemostat and the rates at which it is removed by rotifer ingestion and by being washed out of the system.

Equations governing the states of the algae and rotifer populations are usually stated in terms of the respective volume-normalized mass concentrations  $A(t)$  and  $R(t)$  (dimensions: mass·volume<sup>-1</sup>); e.g.  $R(t) = M(t)/V$ , where  $V$  is the (constant) culture volume. The Monod-Herbert model, for example, can be written in the form:

$$\begin{aligned} \frac{dA}{dt} &= A_0D - AD - \frac{I_{\text{sup}}AR}{K_h + A}, \\ \frac{dR}{dt} &= Y \frac{I_{\text{sup}}AR}{K_h + A} - \rho R - DR, \end{aligned} \quad (1)$$

where the first and second equations specify the instantaneous rates of change in mass concentrations of

algae and rotifers, respectively, and

- $A_0$  =algal mass concentration in the feed;
- $D$  =dilution rate (inflow divided by  $V$ );
- $I_{\text{sup}}$  =asymptotic mass-specific rate of ingestion by rotifers;
- $K_h$  =half-saturation constant for ingestion;
- $Y$  =yield coefficient (rotifer biomass produced per unit algal biomass ingested);
- $\rho$  =mass-specific rate of metabolic loss of rotifer biomass.

The three terms on the right side of the algae equation correspond to algal input, washout, and ingestion by rotifers. The three terms on the right side of the rotifer equation correspond to production of rotifer biomass from ingested algae, metabolic loss of biomass, and washout. The model is shown schematically in Figure 1B.

It is important to note that equation (1) asserts that the dynamics of algal and rotifer mass can be understood and predicted with no knowledge of the internal structure of either population (e.g. age or size structure). Thus, according to (1), if we set up a chemostat with fixed initial masses of algae and rotifers, it should make no difference to the system's short-term dynamics whether the rotifer population consists entirely of eggs (which would not ingest algae, and would neither reproduce nor increase in dry mass), entirely of gravid females (which would ingest algae, reproduce, and possibly increase in dry mass, as well), or of some

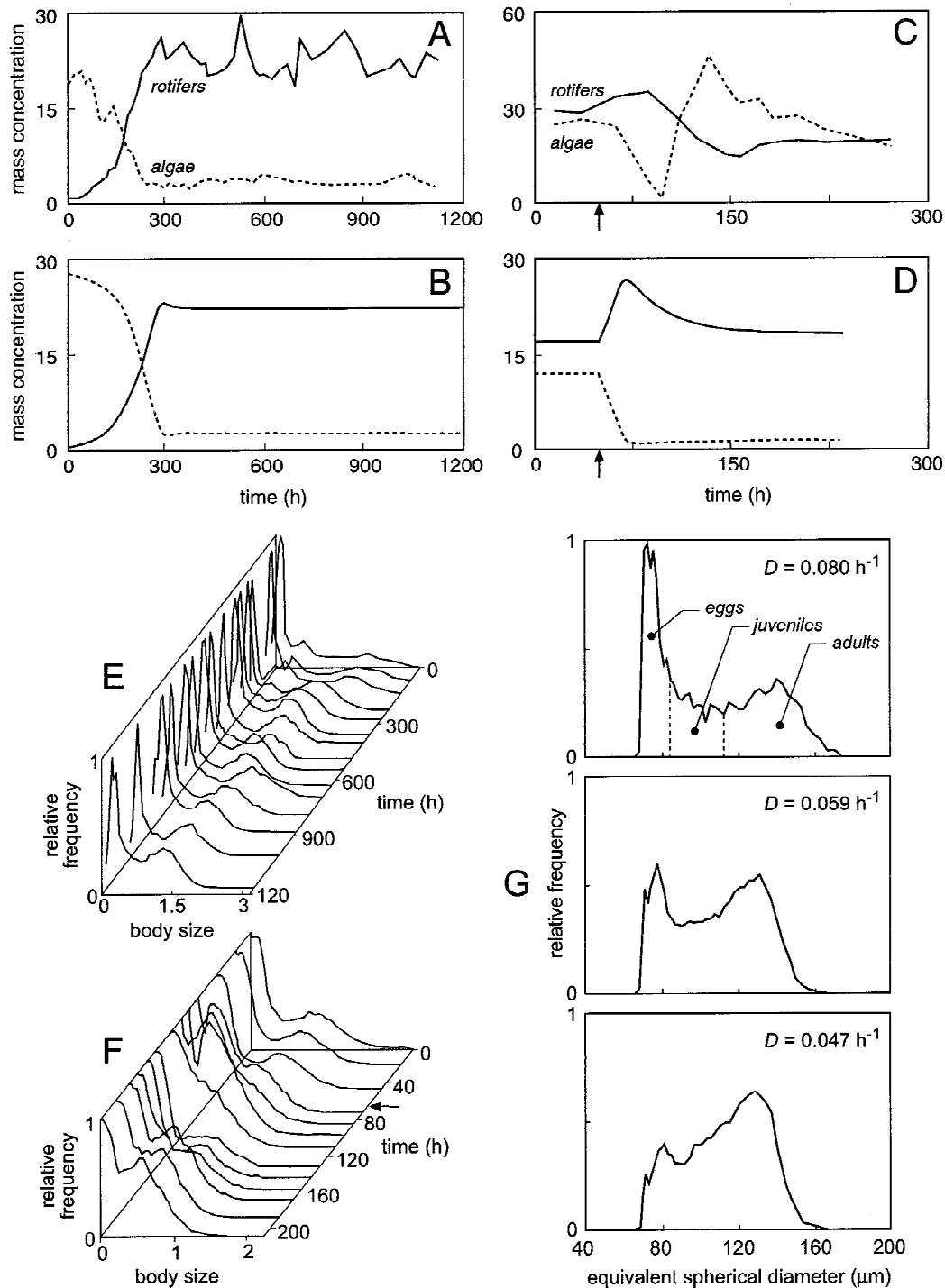


Figure 2. Examples of rotifer chemostat dynamics in laboratory experiments. All examples apply to *Brachionus calyciflorus*. A—Approach to quasi-steady state. Mass concentration units:  $\mu\text{g}\cdot\text{mL}^{-1}$  for rotifers,  $\mu\text{g}\cdot\text{mL}^{-1} \times 5.7$  for algae. B—Dynamics predicted by the Monod-Herbert model for data-series A. Units: same as in A. C—Effect of a downward shift in dilution rate (arrow) following the end of data-series A. Units:  $\mu\text{g}\cdot\text{mL}^{-1}$  for rotifers and algae. D—Dynamics predicted by the Monod-Herbert model for data-series C. Units: same as in C. E, F—Observed dynamics of the rotifer size distribution in data-series A and C. Size distributions are normalized to achieve a constant egg-peak height; non-normalized distributions are shown in Figure 5 of Boraas et al. (this volume). Body size units:  $\mu\text{m}^3 \times 10^6$ . G—Steady-state rotifer size distributions at three different dilution rates. Top distribution shows approximate sizes of eggs, juveniles, and adults. Data: A–F: Boraas (1983), G: Bennett & Boraas (1989).

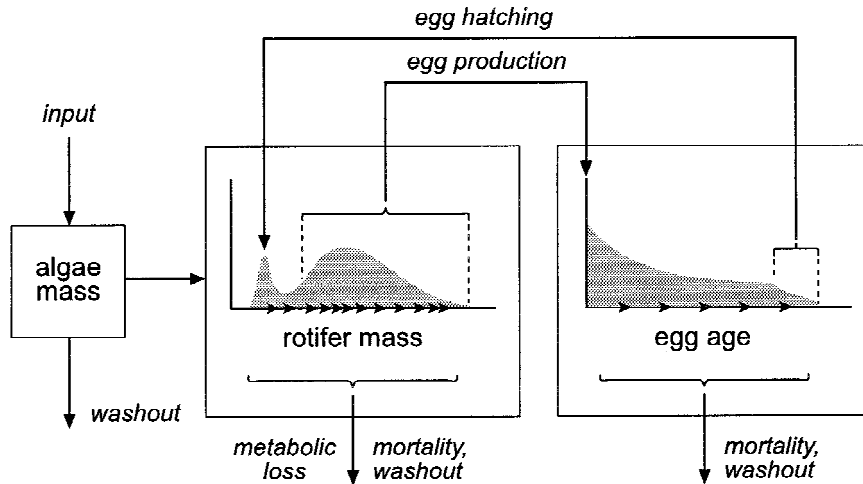


Figure 3. Schematic of the proposed physiologically structured chemostat model. See text for description.

mix of life stages. If this property were to hold for real rotifer chemostats, it would be a most remarkable one, indeed.

### Key experimental evidence

We now show results of several experiments that permit an assessment of classical chemostat models, here represented by the Monod-Herbert model. Figure 2A shows the results of an experiment conducted by Boraas (1983) in which *Brachionus calyciflorus* was introduced into a chemostat at low abundance and allowed to grow. Figure 2B shows the dynamics predicted by a calibrated Monod-Herbert model. Note the contrast between the smooth approach to steady state predicted by the model and the pronounced and persistent fluctuation observed. This result is typical of such experiments (e.g. Rothaupt, 1993; Walz, 1993) and reveals that the Monod-Herbert model exhibits too little tendency toward oscillation, compared to real rotifer populations.

A more striking discrepancy is demonstrated in panels C and D of Figure 2, which show the results of a downward *D*-shift experiment conducted by Boraas (1983). The chemostat was allowed to run for roughly 1000 h at  $D = 0.045 \text{ h}^{-1}$ , after which *D* was abruptly decreased to  $0.0135 \text{ h}^{-1}$  (by reducing the pump speed). As the figure shows, the observed transient dynamics following the downward shift in *D* (panel C) bear little resemblance to the behavior predicted by the calibrated Monod-Herbert model (panel D). Most

notably, the algae showed a dramatic resurgence following their initial crash, whereas the model predicted essentially none. A similarly gross discrepancy was observed by Walz (1993) in a *D*-shift experiment with *Brachionus angularis*.

Another serious problem with classical chemostat models as applied to rotifers is that they are unable to address phenomena dealing with population structure. For example, panels E and F of Figure 2 (from Boraas, 1983) show dynamics of the rotifer size structure corresponding to the mass dynamics in panels A and C. In panel F, note that the *D* shift is followed by loss of the egg peak, accumulation of juveniles and small adults, then return of the egg peak (egg, juvenile, and adult segments of the size distribution are identified in panel G). Another example appears in panel G (from Bennett & Boraas, 1989), which shows the steady-state rotifer size distribution at three different dilution rates. Note that the steady-state egg peak is taller relative to the adult peak at higher dilution rates. Size-structure patterns such as these provide valuable clues about the mechanisms of rotifer population regulation but cannot be addressed using classical models.

Based on the inability of classical chemostat models to account for observed transient dynamics of total mass, and on their inability to address observed patterns in population structure (and also for theoretical reasons beyond the scope of this paper), we believe that these models are inadequate tools for studying the rotifer chemostat. In the next section, we propose a new model that resolves some of these problems.

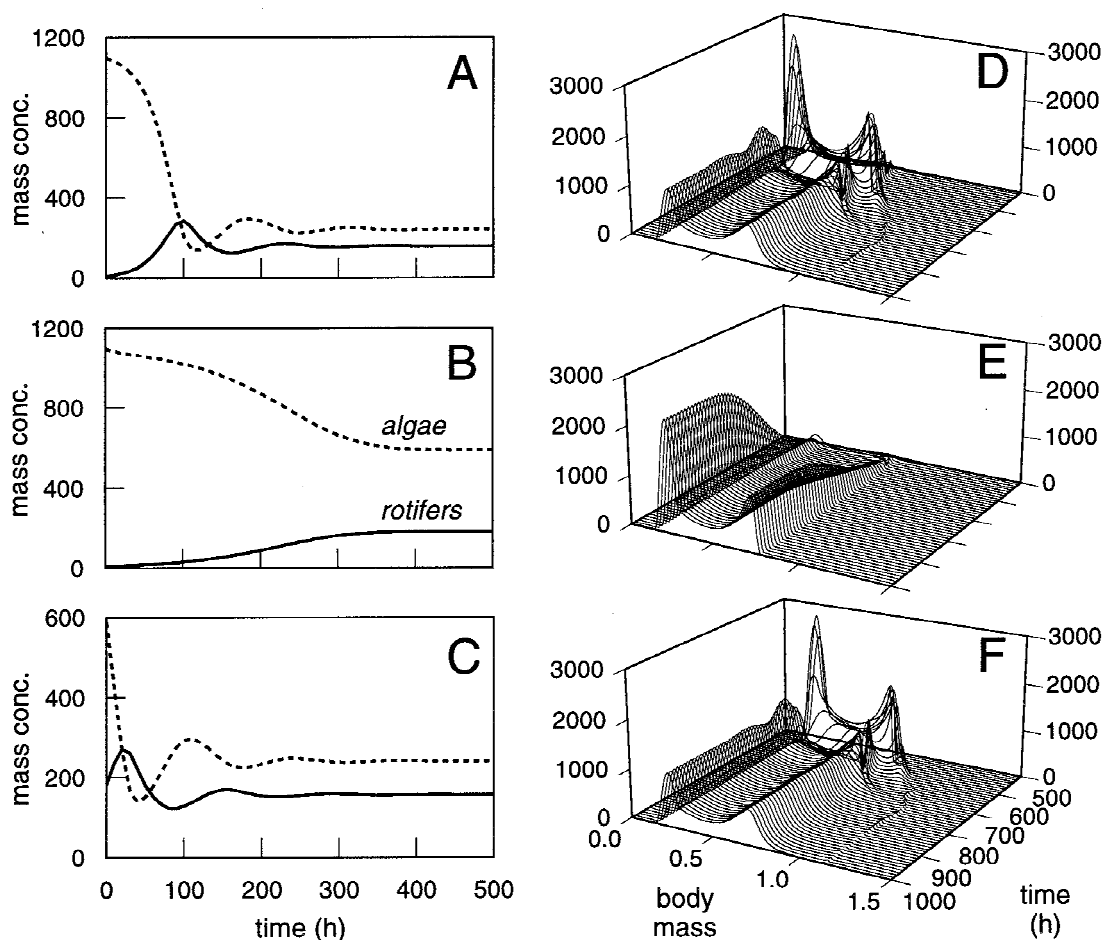


Figure 4. Examples of model dynamics. A—Total algal and rotifer masses at  $D = 0.02 \text{ h}^{-1}$ . B—Total algal and rotifer masses at  $D = 0.05 \text{ h}^{-1}$ . C—Continuation of B after a step-change in dilution rate to  $D = 0.02 \text{ h}^{-1}$ . D—Rotifer size distributions corresponding to A. Vertical axis is population density. E—Rotifer size distributions corresponding to B. F—Rotifer size distributions corresponding to C.

### A simple physiologically structured model

Our objective in developing a new model of the rotifer chemostat was to add the minimum biological detail necessary to account for currently known phenomena, and to increase the correspondence between model components and experimentally measurable properties. We therefore decided to (a) add only a few key components of structure to the rotifer population, (b) focus on structural components that are experimentally measurable and directly related to basic physiological mechanisms, (c) keep the model simple enough so it is both computationally tractable and reasonably transparent to underlying principles, and (d) pose the model in a form that can be reduced to a classical model via specializing assumptions (so the reasons

for differences in model properties can be clearly identified).

The basic idea behind the model is illustrated in Figure 3. Recall from Figure 1B that classical chemostat models can be diagrammed as two (connected) boxes with no internal structure. In the new model, the algae box of the classical model is retained, but two types of structure are added to the rotifer box. First, the population is divided into two discrete stages: eggs and free-swimming rotifers (hereafter, rotifers). Second, each stage is given a different type of continuous internal structure: generalized age for eggs (e.g. degree days) and body mass for rotifers. Thus, the new model is only slightly more complex than classical models and remains biologically quite simple.

The model works as follows. Rotifers continuously ingest algae and consequently grow along the body mass axis (with negative growth allowed). Once a threshold body mass is crossed, they become adults and begin allocating some of their net assimilated mass to egg production. The eggs produced enter the age axis of the egg stage at generalized age 0 and begin a process of development, eventually crossing a threshold age at which they begin to hatch. The neonates produced return to the body mass axis of the rotifer stage, with variability in neonatal body size allowed. The newborn rotifers then begin to grow, and the life cycle is complete.

Using the methods of continuum transport modeling, the schematic of Figure 3 is easily translated into a set of equations comprising an ordinary differential equation governing the algae, a mass-structured hyperbolic partial differential equation (with boundary condition) governing the rotifers, and an age-structured hyperbolic partial differential equation (with boundary condition) governing the eggs:

$$\begin{aligned} \frac{dA}{dt} &= (A_0 - A)D - \varepsilon \int_{x_0}^{\infty} F(A, x)n(t, x) dx \\ \frac{\partial n}{\partial t} + \frac{\partial(\gamma n)}{\partial x} &= b(x) \int_0^{\infty} v(a)n_e(t, a) da \\ &\quad - [\mu(A, x) + D]n(t, x), \quad x > x_0 \\ &\text{subject to } n(t, x_0) = 0 \quad \text{when } \gamma(A, x_0) > 0 \\ \frac{\partial n_e}{\partial t} + u \frac{\partial n}{\partial a} &= -[v(a) + \mu_e(a) + D]n_e(t, a), \\ &\quad a > 0 \\ &\text{subject to } un_e(t, 0) = \int_{x_0}^{\infty} \beta(A, x)n(t, x) dx, \end{aligned} \quad (2)$$

where:

- $A(t)$  = total mass of algae at time  $t$ , per unit volume of culture;
- $n(t, x) dx$  = number of rotifers with body mass between  $x$  and  $x + dx$  at time  $t$ , per unit volume of culture;
- $n_e(t, a) da$  = number of eggs with generalized age between  $a$  and  $a + da$  at time  $t$ , per unit volume of culture;
- $\gamma(A, x)$  = rate of growth in rotifer body mass at body mass  $x$ ;
- $b(x)$  = probability density function for the mass of a rotifer egg;

- $v(a)$  = egg maturation rate at generalized age  $a$ ;
- $\mu(A, x)$  = mortality rate of rotifers at body mass  $x$ ;
- $D$  = dilution rate;
- $u$  = temperature-dependent rate of generalized aging in eggs;
- $\mu_e(a)$  = egg mortality rate at generalized age  $a$ ;
- $A_0$  = input mass concentration of algae;
- $\varepsilon$  = algal cell mass;
- $F(A, x)$  = rotifer ingestion rate at body mass  $x$  (cells per time per rotifer);
- $x_0$  = lower limit of body mass for a rotifer;
- $\beta(A, x)$  = rotifer egg production rate at body mass  $x$ .

Other choices of the boundary condition for the rotifer equation are plausible. All quantities except  $\gamma$  are restricted to being nonnegative, and we assume  $b(x) > 0$  for  $x_1 < x < x_2$ , and  $b(x) = 0$  otherwise (so all egg masses fall within a finite interval).

The rates at which eggs and rotifers are transported along their respective structural axes are determined by the rates of generalized aging and of growth in body mass. For simplicity, we assume in the numerical examples below that generalized aging occurs at a constant rate  $u = 1$ , which is equivalent to chronological aging. Growth in body mass is assumed to be given by the amount of net assimilation (gross assimilation minus metabolic loss) allocated to growth rather than reproduction. The net assimilation rate  $\alpha(A, x)$  is given by

$$\alpha(A, x) = [\varepsilon p(A, x) - \xi(A, x)]F(A, x) - \rho x^\theta,$$

where  $p(A, x)$  = assimilation fraction,  $\xi(A, x)$  = assimilate spent on acquisition and processing, per ingested cell, and  $\rho x^\theta$  = resting metabolic loss rate. Growth and fecundity are then given by

$$\begin{aligned} \gamma(A, x) &= \alpha(A, x)\phi_s(\alpha, x), \\ \beta(A, x) &= \frac{\alpha(A, x)\phi_r(\alpha, x)}{\int yb(y) dy}, \end{aligned}$$

where  $\phi_s(\alpha, x)$  and  $\phi_r(\alpha, x)$  are the proportional allocations to somatic growth and reproduction, and the denominator in the formula for  $\beta(A, x)$  is the average mass of an egg (which converts reproduction from mass of eggs per time to number of eggs per time). Proportional allocation to somatic growth and reproduction are related by

$$\phi_r(\alpha, x) = 1 - \phi_s(\alpha, x),$$

so it suffices to specify only  $\phi_r(\alpha, x)$ .

In the numerical examples below,  $\phi_r(\alpha, x)$  is assumed to be the product of a component depending

only on  $x$  and a component depending only on  $\alpha$ , with allocation working as follows. No net assimilate is allocated to reproduction if body mass is too small (in which case the size-dependent component is zero) or if net assimilation is too small (in which case the assimilation-dependent component is zero). The size-dependent component is constant except in a certain interval on the body-mass axis (the maturation window) over which it increases from the juvenile value ( $= 0$ ) to the adult value. The assimilation-dependent component is zero for negative net assimilation and increases toward a positive asymptote with increasing positive net assimilation. These assumptions are for purposes of illustration and probably will require adjustment in actual applications.

### Numerical examples

We now illustrate the behavior of model (2). Our purpose is merely to show a few types of behavior the model can exhibit, and to compare these with available data in a qualitative and preliminary way. Thorough exploration of the model's properties and accurate estimation of parameter values are major tasks and are beyond the scope of this paper.

Panels A–C in Figure 4 show examples of total-mass dynamics. Panels A and B show the initial behavior and approach to steady state with  $D = 0.02 \text{ h}^{-1}$  and  $D = 0.05 \text{ h}^{-1}$ , respectively. Transient oscillation is evident in A but effectively disappears at high dilution rates, as in B. The dilution rate of example B was shifted downward to  $D = 0.02 \text{ h}^{-1}$  at  $t = 500 \text{ h}$ , and the subsequent dynamics are shown in panel C. Note that the initial crash in algal mass is followed by a pronounced resurgence, which is roughly the behavior observed by Boraas (1983) and Walz (1993) in their laboratory experiments (e.g. Figure 2C). The assimilation-dependent component of the allocation function plays an important role in determining how pronounced this resurgence is.

Panels D–F in Figure 4 show dynamics of the rotifer size structure during the same numerical experiments whose mass dynamics are shown in panels A–C. The size distribution shows transient wave-like oscillations in D, but these disappear at high dilution rates, as in E. Similar oscillations are set off by a downward shift in dilution rate, as shown in panel F. Note in particular the initial loss of the egg peak (as the crash in residual algae causes adults to divert net assimilation away from reproduction), the accumulation of juven-

iles and small adults, then return of the egg peak at a lower height. This is basically the pattern observed by Boraas (1983), shown in Figure 2F above and in Figure 5 of Boraas et al. (this volume). Also note that the steady-state egg peak is higher relative to the adult peak when  $D = 0.05 \text{ h}^{-1}$  (panel E) than when  $D = 0.02 \text{ h}^{-1}$  (panels D, F). This result is consistent with the pattern observed by Bennett & Boraas (1989), shown in Figure 2G.

### Discussion

Our preliminary numerical results suggest that the new model is promising, but final judgement on its value awaits rigorous empirical tests. We expect laboratory experiments to indicate that adjustments in the model are necessary, and we note in this connection that various modifications and embellishments can be made without destroying the model's tractability. For example, accounting for observed chemostat dynamics at low dilution rates may require modeling the accumulation of fecal debris in the culture, since ingestion of this material is likely to alter gross assimilation by rotifers. Or it might be necessary to allow egg size to vary with factors such as maternal body mass or net assimilation rate. Generalized or chronological aging can also be incorporated in the rotifer equation (e.g. if maturation to adulthood must be allowed to depend in part on age, or if senescence is important), though we note that there is no adequate way to measure age in a chemostat.

If experiments indicate that substantially greater biological detail must be incorporated into the model, then it probably will be necessary to abandon the continuum transport modeling framework in favor of a stochastic, individual-based, computer simulation model where the fate of each individual in the rotifer population is tracked separately through time. Such models have fewer computational constraints than continuum transport models, mainly because they avoid the realm of multidimensional partial differential equations and their attendant numerical difficulties. It must be remembered, however, that regardless of the modeling framework employed, including a high degree of biological detail will produce a model whose behavior is largely incomprehensible. Too much detail is therefore as bad as too little in research aimed at elucidating basic principles.

### Acknowledgement

This work was partially funded by a grant to JNM from the Environmental Associates of the Academy of Natural Sciences of Philadelphia.

### References

- Bennett, W. N. & M. E. Boraas, 1989. Comparison of population dynamics between slow- and fast-growing strains of the rotifer *Brachionus calyciflorus* Pallas in continuous culture. *Oecologia* 81: 494–500.
- Boraas, M. E., 1979. Dynamics of Nitrate, Algae, and Rotifers in Continuous Culture: Experiments and Model Simulations. Ph.D. thesis, Pennsylvania State University.
- Boraas, M. E., 1983. Population dynamics of food-limited rotifers in two-stage chemostat culture. *Limnol. Oceanogr.* 28: 546–563.
- Boraas, M. E., D. B. Seale, J. E. Boxhorn & J. N. McNair, 1998. Rotifer size distribution changes during transient phases in open cultures. *Hydrobiologia* 387/388 (Dev. Hydrobiol. 134): 477–482.
- Herbert, D., 1958. Some principles of continuous culture. In G. Tunevall (ed.), *Recent Progress in Microbiology*. Blackwell, London: 381–396.
- Monod, J., 1950. La technique de culture continue; theorie et applications. *Ann. Inst. Pasteur, Lille* 79: 390–410.
- Rothaupt, K. O., 1993. Critical consideration of chemostat experiments. In N. Walz (ed.), *Plankton Regulation Dynamics*. Springer-Verlag, New York: 217–225.
- Walz, N., 1993. Model simulations of continuous rotifer cultures. *Hydrobiologia* 255/256: 165–170.